Structure, energetics, and bonding of amorphous Au–Si alloys

Soo-Hwan Lee and Gyeong S. Hwang[a)]
Department of Chemical Engineering, University of Texas at Austin, Austin, Texas 78712, USA

(Received 12 July 2007; accepted 25 October 2007; published online 13 December 2007)

First principles periodic calculations based on gradient-corrected density functional theory have been performed to examine the structure, energetics, and bonding of amorphous Au–Si alloys with varying Au:Si composition ratios. Our results predict that the Au–Si alloy forms the most stable structure when the Si content is around 40–50 at. %, with an energy gain of about 0.15 eV/atom. In addition, the volume change per atom in the alloy exhibits a distinctive nonlinear trend, with the minimum value around 60 at. % Si. The occurrence of the minimum in the Au–Si mixing energy and volume is attributed to strong hybridization of the Au $5d$–Si $3p$ states. We also present variations in the radial distribution function and atomic coordination number as a function of Au:Si composition ratio, with discussion of the nature of local packing and chemical bonding in the Au–Si alloy system. © *2007 American Institute of Physics*. [DOI: 10.1063/1.2815326]

I. INTRODUCTION

Accurate determination of the atomic structure and physical properties of amorphous metal alloys has long been an issue of great interest not only because of their scientific importance but also of various engineering applications. Earlier studies[1–3] evidenced that the structure of bulk metallic alloys deviates significantly from a simple random packing model,[4,5] while also exhibiting a strong dependence on their chemical composition. The structural parameters of metallic alloys have been commonly determined based on x-ray diffraction measurements; however, interpretation of such data is often uncertain. Under such circumstances, first principles based atomistic modeling has recently emerged as a powerful means to address the structure, function, and physical properties of complex bulk metallic alloys.[6–9]

In this paper, we use first principles quantum mechanical simulations to examine the structural, energetics, and bonding properties of amorphous Au–Si alloys. We first calculate variations in the mixing enthalpy and alloy volume with varying Au:Si composition ratios. Then, the local order in Au–Si alloys is presented using calculation and analysis of the radial distribution function and atomic coordination number. In addition, the nature of local packing in the Au–Si alloy particularly with moderate Si content is discussed. We also discuss the Au–Si bonding mechanism based on density of states analyses.

The binary Au–Si alloy was the first amorphous metal alloy obtained by rapid cooling of the liquid state,[10] but it still remains one of the most puzzling amorphous alloys.[11] A few x-ray based experiments have been performed to examine the Au–Si alloy structure and energetics at selected Au:Si compositions, such as $Au_{81}Si_{19}$ (Ref. 12) and $Au_{75}Si_{25}$ (Refs. 13 and 14) as well as the surface segregation and crystallization of Si in the $Au_{82}Si_{18}$ alloy.[11] Au has been found to be very reactive toward Si, although it is a very stable nonreactive novel metal. Au deposition on a Si surface, therefore, easily leads to silicide formation.[15,16] In addition to the scientific significance of understanding the nature of amorphous metallic alloys, the Au–Si system has recently received great attention because of its technological importance, including growth and self-assembly of Si nanowires,[17] interconnections of Si-based electronic devices,[18] and bonding of nanoelectromechanical devices.[19] Results from the present first principles calculations can be used to complement the existing experimental observations and to clarify microscopic mechanisms underlying the Au–Si alloying during the fabrication and operation of various relevant Si-based devices.

II. COMPUTATIONAL METHOD

The model structures of amorphous Au–Si alloys employed in this work were generated using combined modified embedded atom method[20] (MEAM) and *ab initio* molecular dynamics (MD) simulations in the canonical ensemble. We first performed MEAM-MD simulations at high temperatures (2500 K) in order to obtain the randomized structures of pure Au and Si, starting with their crystalline structures. For each case, 64 atoms were placed in a periodic supercell. Based on the randomized Au and Si structures, we prepared melted Au–Si alloy structures at various compositions by replacing Si with Au or Au with Si, followed by MEAM-MD annealing at 2500 K for 300 ps. Next, the Au–Si alloy structures were further annealed using *ab initio* MD within a Born-Oppenheimer framework at 2500 K for 20 ps with a time step of 1 fs, and then rapidly quenched at a rate of 2.0 K/fs. Here, the temperature was controlled using velocity rescaling. Finally, we refined the quenched structures with careful volume optimization using first principles total energy minimization calculations. While no simulation study has been reported for the Au–Si system, our previous studies[21,22] have demonstrated that the chosen simulation conditions are sufficient for determining the structure of amorphous metal alloys. In addition, our calculations predict that the packing densities of Si and Au in the amorphous

[a)]Author to whom correspondence should be addressed. Telephone: 512-471-4847. Fax: 512-471-7060. Electronic mail: gshwang@che.utexas.edu

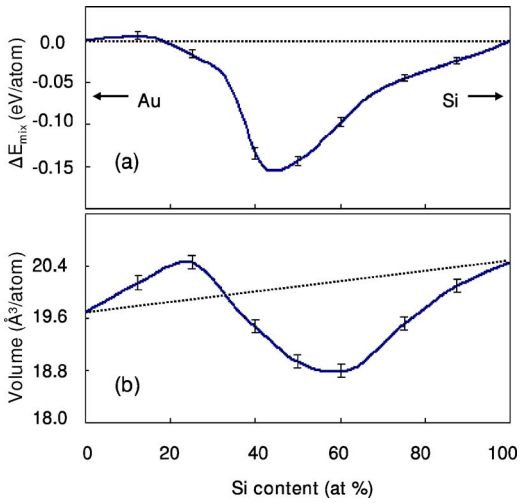

FIG. 1. (Color online) Variations in (a) the predicted mixing enthalpy and (b) alloy volume per atom of amorphous Au–Si alloy as a function of Si content (at. %). The values are based on nine different 64-atom supercell calculations.

state are about 5% and 3% less than their crystalline counterparts, respectively, in good agreement with previous experimental observations.[23,24]

In this work, *ab initio* MD and static structural optimization were performed using the well established plane-wave program VASP.[25–27] We used the generalized gradient approximation derived by Perdew and Wang[28] to density functional theory. A plane-wave basis set for valence electron states and Vanderbilt-type ultrasoft pseudopotentials[29,30] for core-electron interactions were employed. A plane-wave cutoff energy of 270 eV was used and the Brillouin zone integration was performed using one k point (at Gamma). We checked carefully the convergence of atomic configurations and relative energies with respect to plane-wave cutoff energy and k point. All atoms were fully relaxed using the conjugate gradient method until residual forces on constituent atoms become smaller than 5×10^{-2} eV/Å.

III. RESULTS AND DISCUSSION

Figure 1(a) shows a variation in the enthalpy of mixing as a function of Au:Si composition ratio, with respect to pure amorphous Au and Si. Here, the mixing enthalpy per atom (ΔE_{mix}) is given by

$$\Delta E_{\mathrm{mix}} = E(\mathrm{Au}_{1-x}\mathrm{Si}_x) - (1-x)E_{\mathrm{Au}} - xE_{\mathrm{Si}},$$

where $E_{\mathrm{Au-Si}}$ is the total energy per atom of the Au–Si alloy examined, x is the number fraction of Si in the Au–Si alloy, and E_{Au} and E_{Si} are the total energies per atom of pure amorphous Au and Si, respectively. The result shows that the Au–Si alloy forms the most stable structure when the Si content is around 40–50 at. %, with an energy gain of about 0.15 eV/atom. Our value is consistent with 0.31 eV (=30 kJ/mol) per Au–Si pair as estimated for the $Au_{50}Si_{50}$ alloy based on Miedema's model of Takeuchi and Inoue.[31] The sizable negative mixing enthalpy suggests that Au and Si materials can easily be alloyed together, which is consistent with the experiments.[32,33] It is also worth noting that the mixing enthalpy becomes slightly positive when the Si content is small, which might indicate the presence of a barrier for incorporation of Si into pure Au.

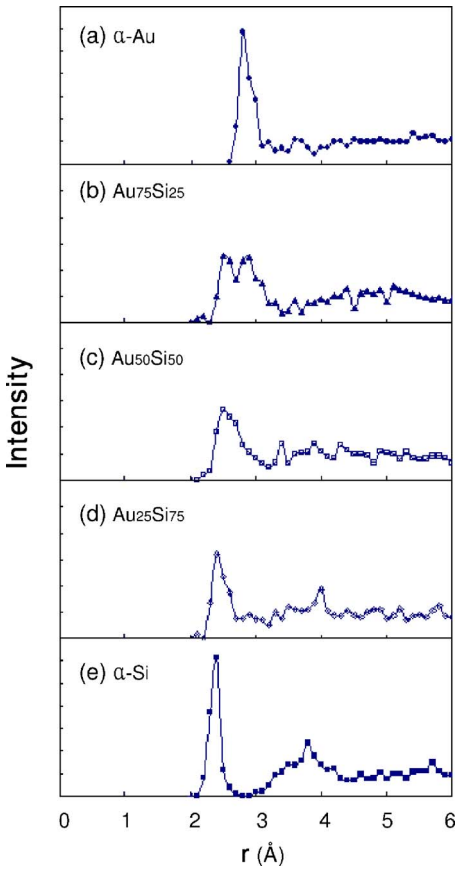

FIG. 2. (Color online) Total radial distribution functions for amorphous Au–Si alloys at selected Au:Si composition ratios as well as pure amorphous Au and Si as indicated. The values are obtained based on three different 64-atom supercell calculations.

Figure 1(b) shows the predicted volume change per atom of the amorphous Au–Si alloy as a function of Si content. The volume change exhibits a distinctive nonlinear trend. When the Si content is relatively small (<20–30 at. %), the volume slightly increases with Si content. However, as more Si is added the volume gradually decreases and yields the minimum value at 60 at. % Si, which also indicates a strong interaction between Au and Si atoms in the amorphous Au–Si alloy.

Figure 2 shows the total radial distribution functions for the Au–Si alloy at selected Au:Si compositions, along with the pure amorphous Au and Si cases. The total radial distribution function $g(r)$ was computed using three different 64-atom supercells for good statistics. For the pure Au (a) and Si (e) structures, the distinct and narrow first peaks appear at around 2.4 and 2.8 Å, respectively, which are in good agreement with the earlier theoretical results.[14,34] As shown in Fig. 2(b), the total $g(r)$ of the $Au_{75}Si_{25}$ structure exhibits two distinct peaks at 2.4 and 2.8 Å, which are well separated from the remaining parts. The first peak is attributed to a combination of Si–Si and Au–Si pairs, whereas the second peak mainly originates from Au–Au correlation. Hence, as the Si content increases, the first peak becomes stronger while the second peak dwindles [(c) and (d)]. Despite the overall metallic character of the Au–Si alloys considered, we

TABLE I. Average and standard deviation (in parenthesis) of the calculated coordination number of Si and Au as a function of cutoff radius. Here, the cutoff radius (r^*) is normalized with respect to 2.5 Å. The upper insets show the simulated structures of Au, $Au_{50}Si_{50}$ alloy, and Si in the amorphous state. The large (gold) and small (green) balls represent Au and Si atoms, respectively.

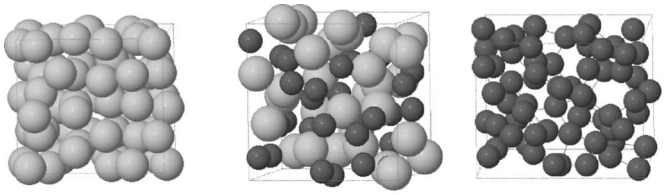

		Coordination number				
		$r^*=1.1$	$r^*=1.2$	$r^*=1.3$	$r^*=1.4$	$r^*=1.5$
Pure Au		1.6(0.8)	7.0(0.9)	8.8(0.93)	9.8(0.95)	11.2(0.99)
$Au_{75}Si_{25}$	Si	5.5(0.93)	6.4(0.95)	7.2(0.94)	7.7(1.15)	8.7(1.07)
	Au	2.2(0.99)	5.6(1.16)	7.5(1.22)	8.7(1.25)	9.9(1.27)
$Au_{50}Si_{50}$	Si	4.7(0.76)	5.6(0.83)	6.3(0.92)	7.9(1.27)	10.1(1.51)
	Au	3.3(0.85)	5.7(1.03)	7.0(1.08)	8.8(1.39)	10.5(1.34)
$Au_{25}Si_{75}$	Si	4.3(0.58)	4.8(0.81)	5.5(1.19)	7.3(1.43)	9.7(1.66)
	Au	3.6(0.94)	4.9(0.86)	6.2(0.90)	7.8(1.23)	9.6(1.59)
Pure Si		4.0(0.3)	4.0(0.3)	4.4(0.57)	5.7(1.39)	8.4(2.01)

can expect that the Au–Si distance is shortened to a certain degree as a result of the strong hybridization between Si 3*p* and Au 5*d* orbitals (*vide infra*).

As summarized in Table I, we calculated the average and standard deviation for the coordination number (CN) of Si and Au atoms at selected Au–Si alloys as a function of normalized cutoff radius (r^*). Here, the cutoff radius is normalized with respect to 2.5 Å as obtained for the average nearest neighbor (NN) Au–Si distance from the Au–Si alloys considered. With increasing r^*, the average CN increases while the CN distribution becomes broader as indicated by higher standard deviation. The results also clearly show that the pure Au is more closely packed than the pure Si in the amorphous phase. As also illustrated in the insets, indeed, the amorphous Au structure exhibits a dense random hard-sphere packing, while the amorphous Si structure shows a rather loose continuous random network of covalently bonded atoms. Therefore, in general, a Si rich alloy yields a lower packing density than a Au rich alloy, as evidence by the larger CN of $Au_{75}Si_{25}$ than $Au_{25}Si_{75}$. With a high Si content, indeed, the Au–Si alloy exhibits a more open liquid structure due to the increasing influence of covalentlike Si–Si bonds, which is consistent with the earlier experimental observations.[15] However, the CN of $Au_{50}Si_{50}$ is somewhat greater than those of $Au_{75}Si_{25}$ and $Au_{25}Si_{75}$, particularly when r^* is sufficiently large (>1.5). This is apparently attributed to the relatively higher $Au_{50}Si_{50}$ packing density, as demonstrated by its relatively smaller volume per atom [see Fig. 1(b)]. Our calculations also show that for each Au–Si alloy, the composition ratio within a given value of r^* remains nearly unchanged as the value of r^* varies. This implies that the Au and Si atoms are overall well mixed with no segregation, which can also be seen in the $Au_{50}Si_{50}$ structure (upper inset).

As shown in Fig. 3, the $Au_{75}Si_{25}$ structure also demonstrates that the Au–Si alloy with a moderate Si content results in a glassy structure exhibiting a distinct topological and strong chemical short-range order. Here, the solute Si atoms are more or less evenly distributed while surrounded by Au atoms. The formation of "quasiequivalent" Si-centered Au clusters arising from the strong short-range order also leads to the medium-range order when the clusters are packed in three-dimensional space. In fact, the short-to-medium range order is often seen in transition metal-metalloid systems, where the chemical short-range order is typically significant. The type of the coordination polyhedron around a solute atom can further be specified using the Voronoi index $\langle i_3, i_4, i_5, i_6, \ldots \rangle$, where i_n represents the num-

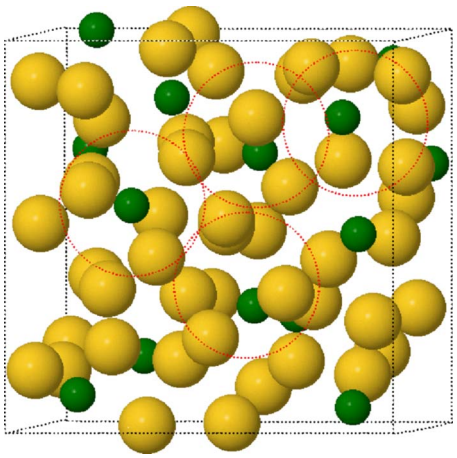

FIG. 3. (Color online) Simulated result for the packing of Si-centered Au polyhedra for a $Au_{75}Si_{25}$ alloy. Large (gold) and small (green) balls represent Au and Si atoms, respectively.

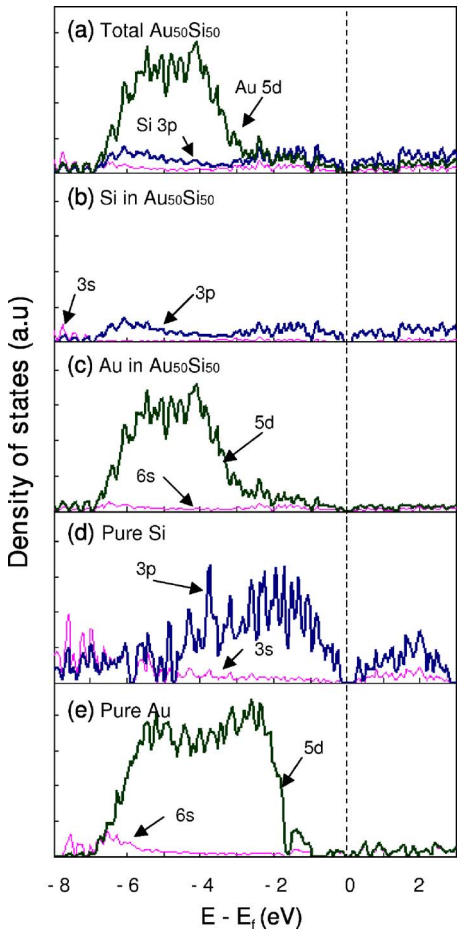

FIG. 4. (Color online) Density of states (DOS) of the $Au_{50}Si_{50}$ structure, (a) total DOS, (b) partial DOS projected on Au, (c) partial DOS projected on Si, together with total DOS of (d) amorphous Si, and (e) amorphous Au, as indicated. The dotted line indicates the Fermi level position.

ber of n-edged faces of the Voronoi polyhedron.[35,36] For the $Au_{75}Si_{25}$ structure, within a cutoff distance of 2.8 Å, the solute coordination polyhedra preferably form the tri-capped trigonal prism Kasper polyhedra, with a Veronoi index of $\langle 0,3,6,0\rangle$. The local order in amorphous binary alloys is mainly governed by the effective atomic size ratio between solvent and solute atoms λ. For instance, an earlier computational study[37] showed that the preferred polyhedra type changes with λ from icosahedral with Voronoi index $\langle 0,0,12,0\rangle$ ($\lambda \approx 0.90$) to bicapped square Archimedean antiprism with $\langle 0,2,8,0\rangle$ ($\lambda \approx 0.84$), and then to tricapped trigonal prism packing with $\langle 0,3,6,0\rangle$ ($\lambda \approx 0.73$). This is consistent with our simulation results considering the smaller atomic size of Si than that of Au. While only considering Au–Si bulk alloys in this work, we expect that their atomic structure would be different from the structure of thin silicide layers formed at the Au/Si interface,[20] and/or surface alloys created by introducing Si to Au surfaces or vice versa.[11] A further investigation into the surface and interface effects is underway.

Finally, to gain understanding of the Au–Si bonding properties, as shown in Fig. 4, we analyzed the density of states (DOS) of the $Au_{50}Si_{50}$ structure, including the total DOS (a) and the partial DOS of Au 5d and 6s (b) and Si 3s and 3p (c). For the sake of comparison, the total DOS of

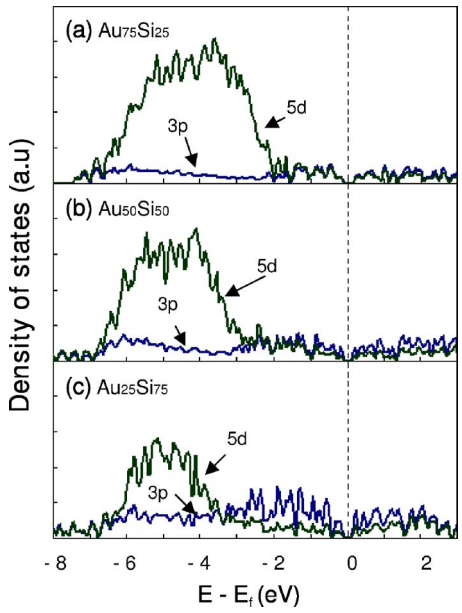

FIG. 5. (Color online) Local density of states (LDOS) projected on Au and Si for (a) $Au_{75}Si_{25}$, (b) $Au_{50}Si_{50}$, and (c) $Au_{25}Si_{75}$. The dotted line indicates the Fermi level position.

pure amorphous Au and Si are also presented in Fig. 4. The Fermi level is used as the reference energy state (which is set to be zero). For pure Au (e), the large and small peaks below −1.5 eV are assigned to the Au 5d and 6s states, respectively, while the states above are free-electron-like. The DOS of amorphous Si shows the p-state peaks mostly above −4 eV, while exhibiting a distinct band gap as expected. Unlike the pure amorphous Si (d), the calculated total DOS of $Au_{50}Si_{50}$ (a) shows no gap at the Fermi level, indicating that the $Au_{50}Si_{50}$ alloy is metallic. The peaks of occupied state densities above −7 eV in the total DOS mainly originate from the Si 3p and Au 5d orbitals. The partial DOS plots [(b) and (c)] clearly demonstrate that, compared to their pure counterparts, there is a significant shift in the Si 3p and Au 5d states to a lower-energy level as a result of a high degree of p-d hybridization in the energy range between −5 and −7 eV. It is apparent that the hybridization of Si 3p with Au 5d states mainly contributes to stabilizing the Au–Si alloy structure. Figure 5 shows a variation in the partial DOS of Au 5d and Si 3p for various Au–Si alloys, demonstrating how the degree of p-d hybridization changes with the Au–Si composition ratio. As expected, the Au–Si p-d hybridization gets stronger as the Au and Si amounts become comparable, explaining the occurrence of the minimum in the Au–Si mixing energy and volume around 50 at. % Si as demonstrated earlier.

IV. SUMMARY

We present the structural, energetics, and bonding properties of amorphous Au–Si alloys based on gradient corrected density functional theory calculations. Our calculations predict that the Au–Si alloy yields the lowest mixing enthalpy (≈0.15 eV/atom) when the Si content is around 40–50 at. %. In addition, we find that the alloy volume slightly increases with Si content when the Si content is rela-

tively small (<20–30 at. %); however, as more Si is added, the volume gradually decreases and yields the minimum value at 60 at. % Si. The occurrence of the minimum in the Au–Si mixing enthalpy and volume indicates a strong interaction between Au and Si atoms. Indeed, our calculation of the density of states of the Au–Si system shows that there is a strong hybridization between the Au 5*d* and Si 3*p* states, which is mainly responsible for the alloy structure stabilization, and that the *d*-*p* hybridization gets stronger as the Au and Si amounts become comparable. Our calculation of the radial distribution function and atomic coordination number also shows that $Au_{50}Si_{50}$ is more closely packed than $Au_{75}Si_{25}$, and $Au_{25}Si_{75}$, while the Si rich alloy ($Au_{25}Si_{75}$) yields a lower packing density than the Au rich alloy ($Au_{75}Si_{25}$). The results also demonstrate that Au and Si atoms are overall well mixed with no segregation. This is apparently attributed to the strong Au–Si interaction. We also find that the Au–Si alloy with a moderate Si content results in a glassy structure exhibiting a distinct topological and strong chemical short-range order, which further leads to the medium-range order when the quasiequivalent Si-centered Au clusters are packed in three-dimensional space. The improved understanding will assist in not only understanding the nature of amorphous metallic alloys but also in explaining and predicting the Au–Si alloying dynamics and interfacial interactions during fabrication and operation of various relevant Si-based devices.

ACKNOWLEDGMENTS

We acknowledge National Science Foundation (CAREER-CTS-0449373) and Robert A. Welch Foundation (F-1535) for their financial support. All our calculations were performed using supercomputers in Texas Advanced Computing Center at the University of Texas at Austin.

[1] S. E. Rodriguez and C. J. Pings, J. Chem. Phys. **42**, 2435 (1965).
[2] P. H. Gaskell, Nature (London) **276**, 484 (1978).
[3] D. B. Miracle and O. N. Senkov, J. Non-Cryst. Solids **319**, 174 (2003).
[4] G. David Scott, Nature (London) **188**, 908 (1960).
[5] J. D. Bernal and J. Mason, Nature (London) **188**, 910 (1960).
[6] R. V. Kulkarni and D. Stroud, Phys. Rev. B **62**, 4991 (2000).
[7] R. V. Kulkarni and D. Stroud, Phys. Rev. B **57**, 10476 (1998).
[8] C. Massobrio, A. Pasquarello, and R. Car, Phys. Rev. B **64**, 144205 (2001).
[9] M. Ji and X. G. Gong, J. Phys.: Condens. Matter **16**, 2507 (2004).
[10] P. A. Garrett, Nature (London) **187**, 869 (1960).
[11] O. G. Shpyrko, R. Streitel, V. S. K. Balagurusamy, A. Y. Grigoriev, M. Deutsch, B. M. Ocko, M. Meron, B. Lin, and P. S. Pershan, Science **313**, 77 (2006).
[12] H. S. Chen and D. Turnbull, J. Appl. Phys. **38**, 3646 (1967).
[13] R. M. Waghorne, V. G. Riylin, and G. I. Williams, J. Phys. F: Met. Phys. **6**, 147 (1976).
[14] X. Bian, J. Qin, X. Qin, Y. Wu, C. Wang, and M. Thompson, Phys. Lett. A **359**, 718 (2006).
[15] J. J. Yeh, J. Hwang, K. Bertness, D. J. Friedman, R. Cao, and I. Lindau, Phys. Rev. Lett. **70**, 3768 (1993).
[16] S. L. Molodtsov, C. Laubschat, and G. Kaindl, Phys. Rev. B **44**, 8850 (1991).
[17] J. B. Hannon, S. Kodambaka, F. M. Ross, and R. M. Tromp, Nature (London) **440**, 69 (2006).
[18] L. J. Lauhon, M. S. Gudiksen, D. Wang, and C. M. Lieber, Nature (London) **420**, 57 (2002).
[19] Y. T. Cheng, L. W. Lin, and K. Najafi, J. Microelectromech. Syst. **9**, 3 (2000).
[20] C. L. Kuo and P. Clancy, Surf. Sci. **551**, 39 (2004), and references therein.
[21] J. H. Shin, A. Waheed, W. A. Winkenwerder, H. W. Kim, K. Agapiou, R. A. Jones, G. S. Hwang, and J. G. Ekerdt, Thin Solid Films **515**, 5298 (2007).
[22] J. H. Shin, A. Waheed, K. Agapiou, W. A. Winkenwerder, H. W. Kim, R. A. Jones, G. S. Hwang, and J. G. Ekerdt, J. Am. Chem. Soc. **128**, 16510 (2006).
[23] P. Mangin, G. Marchal, C. Mourey, and C. Janot, Phys. Rev. B **21**, 3047 (1980).
[24] R. Mosseri, C. Sella, and J. Dixmier, Phys. Status Solidi A **52**, 475 (1979).
[25] G. Kresse and J. Hafner, Phys. Rev. B **47**, 558 (1993).
[26] G. Kresse and J. Furthmüller, Comput. Mater. Sci. **6**, 15 (1996).
[27] G. Kresse and J. Furthmüller, Phys. Rev. B **54**, 11169 (1996).
[28] J. Perdew, J. Chevary, S. Vosko, K. Jackson, M. Pederson, D. Singh, and C. Fiolhais, Phys. Rev. B **46**, 6671 (1992).
[29] D. Vanderbilt, Phys. Rev. B **41**, 7892 (1990).
[30] G. Kresse and J. Hafner, J. Phys.: Condens. Matter **6**, 8245 (1994).
[31] A. Takeuchi and A. Inoue, Mater. Trans. **46**, 2817 (2005), and references therein.
[32] M. Hanbucken, Z. Imam, J. J. Metois, and G. Le Lay, Surf. Sci. **162**, 628 (1985).
[33] H. Dallaporta and A. Cros, Surf. Sci. **178**, 64 (1986).
[34] U. Mizutani, T. Ishizuka, and T. Fukunaga, J. Phys.: Condens. Matter **9**, 5333 (1997).
[35] J. L. Finney, Proc. R. Soc. London, Ser. A **319**, 479 (1970).
[36] J. L. Finney, Nature (London) **266**, 309 (1977).
[37] H. W. Sheng, W. K. Luo, F. M. Alamgir, J. M. Bai, and E. Ma, Nature (London) **439**, 419 (2006).